Supporting Information

High-capacity 1,2:3,4-dibenzophenazine anode integrated into carbon felt for aqueous organic flow battery in alkaline media

Determination of charge transfer rate constant for DBPZ

Fig. S1a shows CVs of DBPZ electrode in 1 M KOH solution at different scan rates. The peak currents are linearly increased with the increase of the square root of the scan rates when the scan rate is higher than 0.2 V s^{-1}(**Fig. S1b**), revealing the characteristic of diffusion-controlled process at high scan rates. The chronoamperometry curves (**Fig. S2a**) were recorded and fitted to determine the diffusion coefficients using the following semi-infinite linear diffusion Cottrell equation [S1]:

$$\boldsymbol{j = nFC_s(\frac{D}{\pi t})^{1/2}} \quad \text{(S1)}$$

where D is the diffusion coefficient, j is the current density, t is time, n is the number of transferred electrons, F is the Faraday constant and C_s is the concentration of redox species within the electrode layer. The concentration (C_s) of redox species is calculated by the equation [S2] as follow:

$$\boldsymbol{C_s = \frac{m}{M_w A \delta}} \quad \text{(S2)}$$

where m is the mass of DHPZ (5.58 μg), M_w is the molecular weight of DHPZ (280.3 g mol^{-1}), A is the geometric area of electrode (0.0707 cm^2) and δ is the average thickness of DBPZ electrode layer that was obtained using a Dektak step profiler

(3.20 μm, **Table S1**). Therefore, the C_s value was calculated to be about 0.88 mol L^{-1}.

According to the linear dependence of j versus $t^{-1/2}$ for the Cottrell plots (**Fig. S2b-S2c**), the D values of the oxidation and reduction progress are calculated to be 1.29×10^{-11} and 1.21×10^{-11} cm^2 s^{-1}, respectively. Therefore, an average D value is found to be 1.25×10^{-11} cm^2 s^{-1}. The charge transfer rate constant (k^0) can be determined using Nicholson's method [S3]. Firstly, the kinetic parameter Ψ was obtained from the potential gap between the oxidation and reduction peak (ΔE_p) using the following equation:

$$\boldsymbol{\Psi = (-0.6288 + 0.0021\Delta E_p)/(-0.017\Delta E_p + 1)} \quad \text{(S3)}$$

Then, k^0 was calculated according to the linear relationship between Ψ and $v^{-1/2}$ shown in the equation (S4).

$$\boldsymbol{\Psi = k^0\left(\frac{\pi DnF}{RT}\right)^{-1/2}v^{-1/2}} \quad \text{(S4)}$$

Therefore, the k^0 was calculated to be 3.7×10^{-3} cm s^{-1}, from the slope of the Ψ~$v^{-1/2}$ dependence (**Fig. S3**).

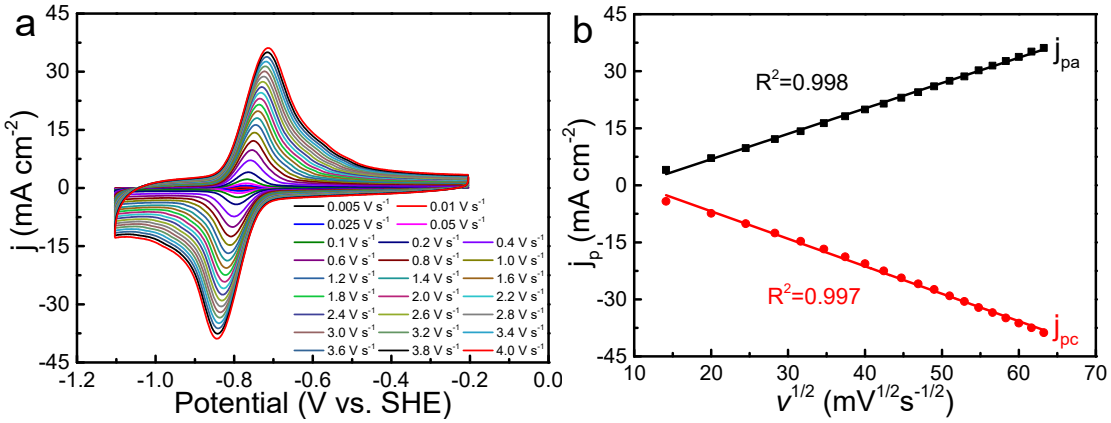

Fig. S1. (a) CVs of DBPZ electrode in 1 M KOH solution at different scan rates (the scan rates (v) from 0.005 to 4 V s^{-1}). (b) Plots of peak current density (j_p) versus square root of scan rate ($v^{1/2}$).

Table S1. Thickness data of the DBPZ electrode layer obtained from Bruker Dektak step profiler.

No.	1	2	3	4	5	6	7	Average value
Thickness (μm)	3.23	3.21	3.17	3.22	3.13	3.20	3.24	3.20

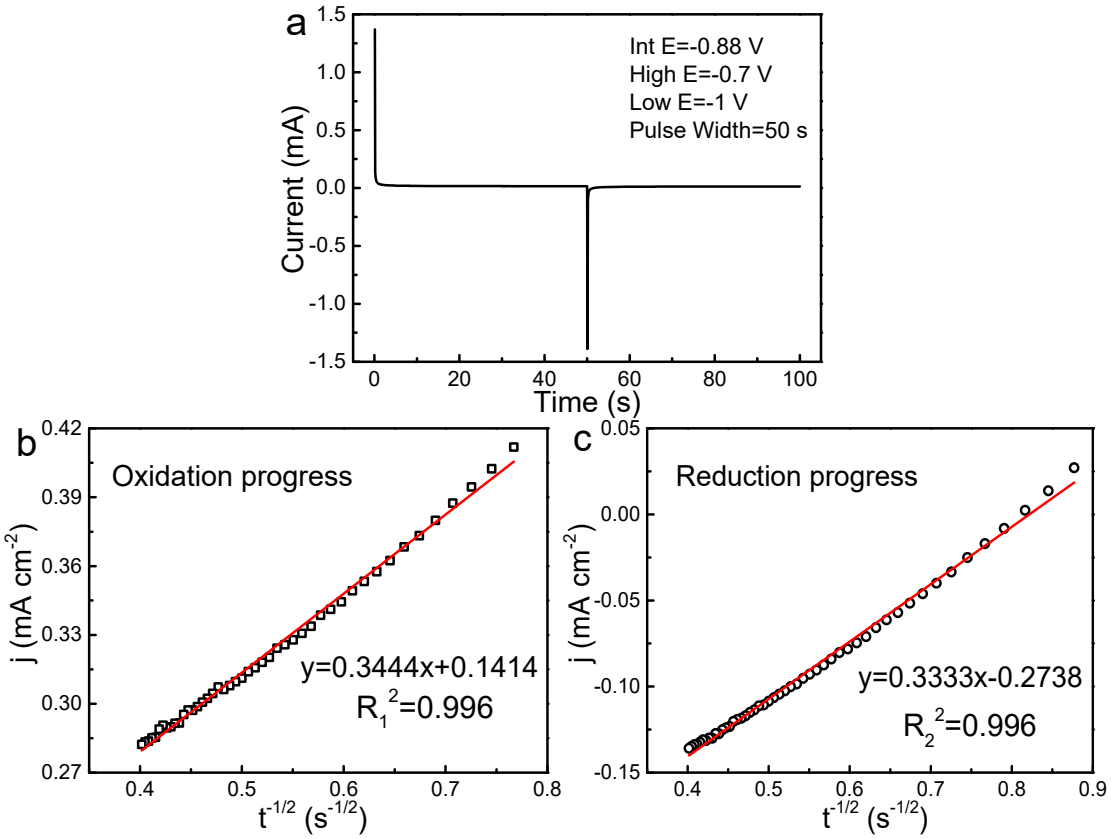

Fig. S2. (a)The chronoamperometry curve of DBPZ electrode in 1 M KOH solution. (b) Cottrell plot for the oxidation reaction. (c) Cottrell plot for the reduction reaction. The results of the linear regression are also shown.

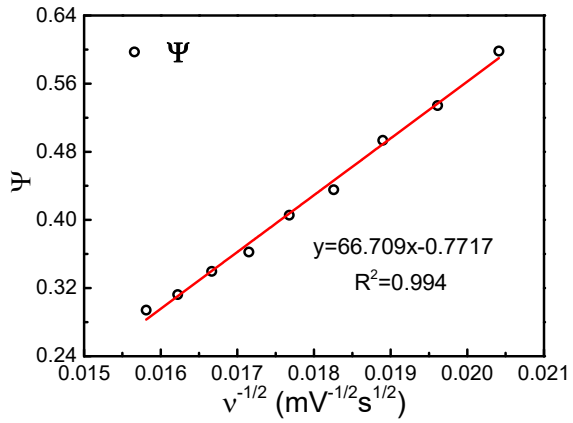

Fig. S3. (a) Plot of Ψ versus $v^{-1/2}$ for DBPZ (The linear relationship was shown with scan rates of 2.4~4.0 V s^{-1}).

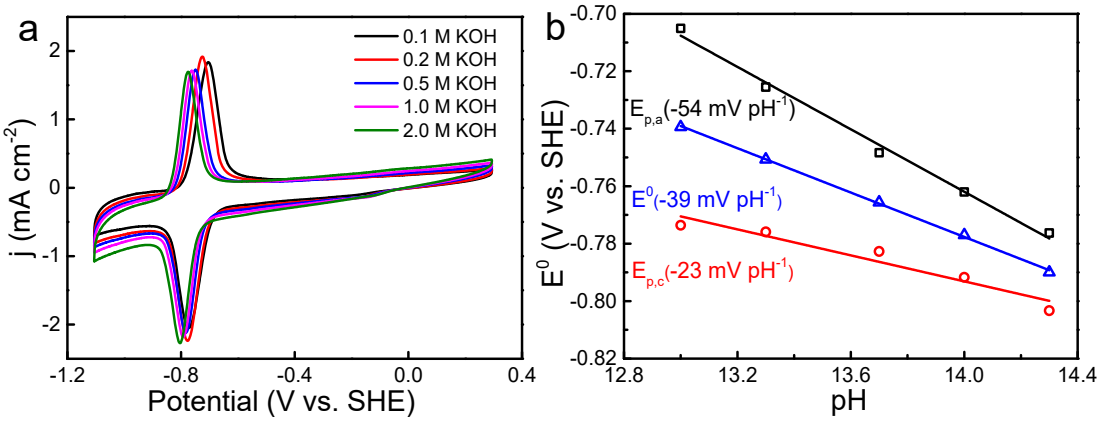

Fig. S4. (a) CVs of DBPZ electrode in KOH solutions of various concentrations at 100 mV s^{-1}. (b) The corresponding Pourbaix diagram.

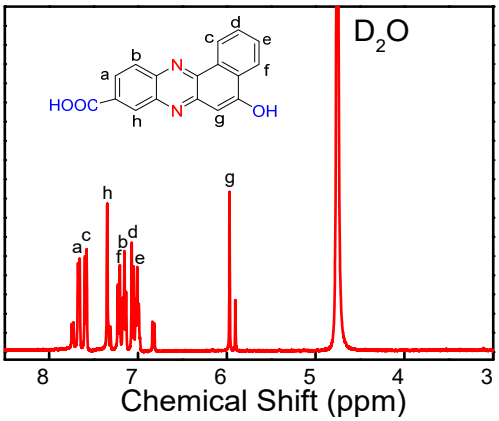

Fig. S5. ^{1}H NMR (300 MHz, $CDCl_3$) spectrum of BHPC. δ 7.68 (m, 1H), 7.58 (d, *J* =7.95 Hz, 1H), 7.35 (d, *J* =1.84 Hz, 1H), 7.22 (dd, *J* =8.7, 1.8 Hz, 1H), 7.15 (t, *J* =7.53 Hz, 1H), 7.07 (d, *J*=8.7 Hz, 1H), 7.01 (t, *J* =7.2 Hz, 1H), 5.97 ppm (s, 1H).

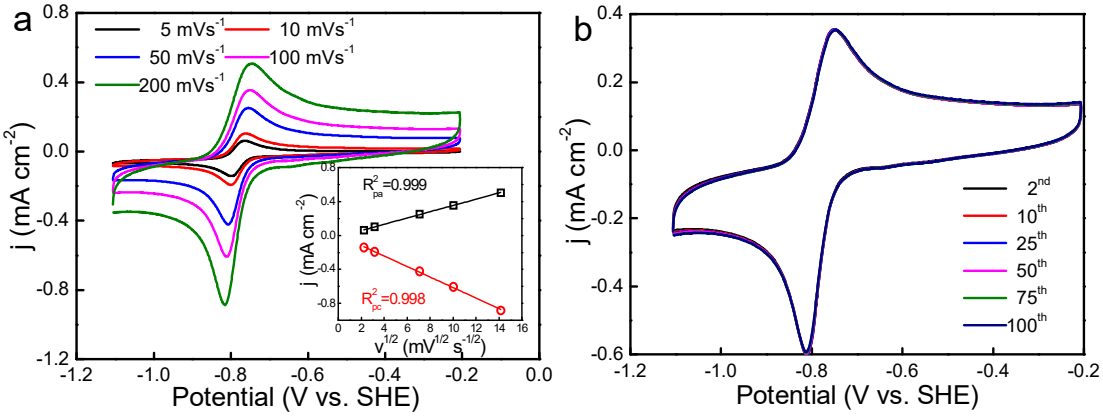

Fig. S6. (a) CVs of BHPC (1 mM) in 1 M KOH solution on a glassy carbon electrode at different scanrates. The inset of (a) is the plot of the current density versus square root of the scan rates ($v^{1/2}$) for BHPC. (b) CVs of BHPC (1 mM) in 1 M KOH solution at 100 mV s^{-1} during the 2nd, 10th, 25th, 50th, 75th and 100th cycles.

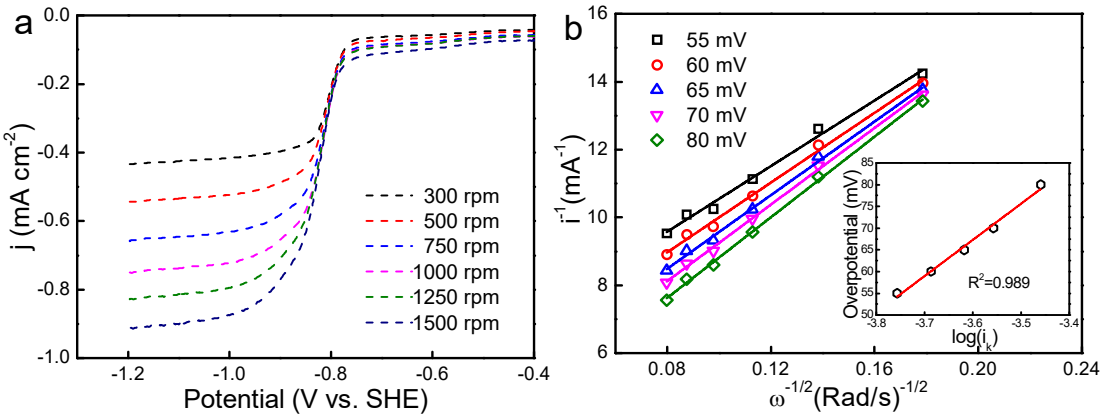

Fig. S7. (a) RDE voltammetry curves of BHPC (1 mM) in 1 M KOH solution on a glassy carbon electrode at 6 rotation rates ranging from 300 to 1500 rpm. (b) Koutecký-Levich plots derived from RDE data at five different BHPC reduction overpotentials. The inset of (b) is the fitted curve of Butler-Volmer equation for BHPC using the kinetic current density (i_k) obtained from the zero-intercept of Koutecký-Levich plots.

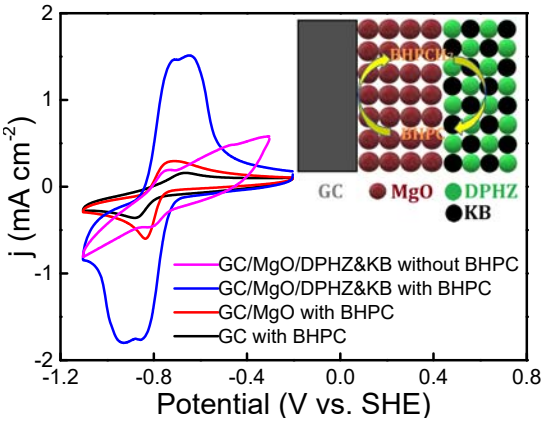

Fig. S8 CV curves in 1 M KOH solution with or without 1 mM BHPC at a scan rate of 50 mV s^{-1}. The working electrode was glassy carbon (GC) coated with porous MgO or MgO/DPHZ&KB layer. The counter and reference electrodes for CV measurements were Pt foil and MMO, respectively. The inset shows the double-layer working electrode structure and the associated redox-targeting reactions. The porous MgO was obtained according to the preparation method reported previously by P. Zhu et al. [S4].

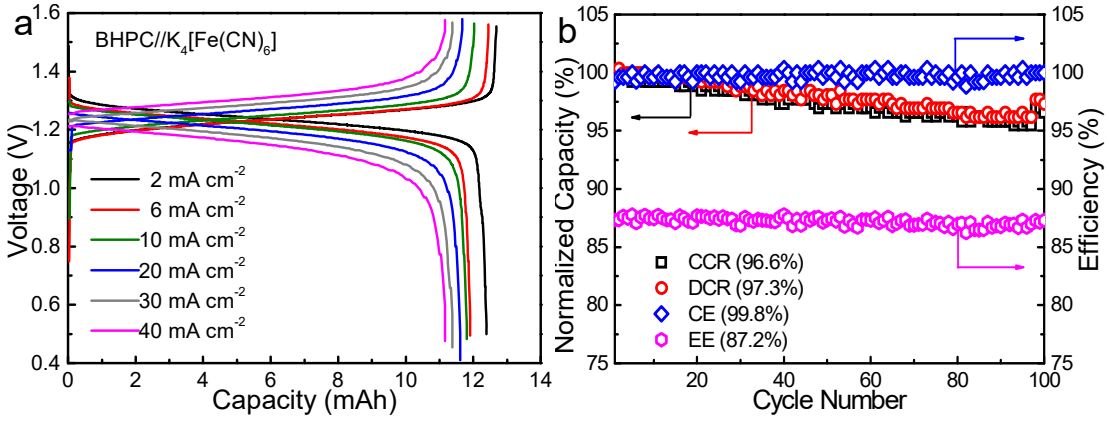

Fig. S9. (a) Galvanostatic charge-discharge profiles of the BHPC//$K_4[Fe(CN)_6]$ ARFB at different current densities. (b) Cycling capacity retention and efficiency data at 30 mA cm^{-2} for the BHPC//$K_4[Fe(CN)_6]$ ARFB. 5 mL 0.05M BHPC + 1 M KOH was used as the anolyte while 10 mL 0.1 M $K_4[Fe(CN)_6]$ + 1 M KOH was used as the catholyte.

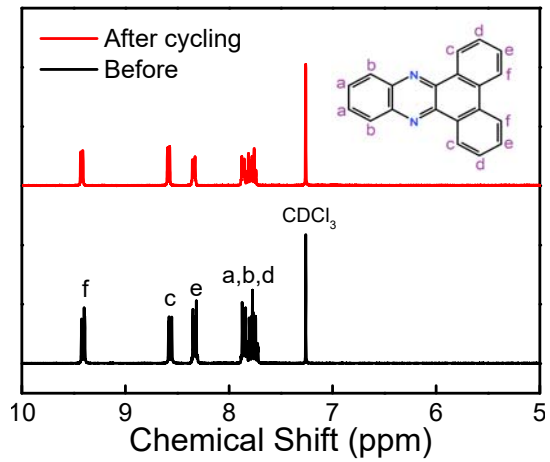

Fig. S10. ^{1}H NMR (300 MHz, $CDCl_3$) spectra of DBPZ employed in the DBPZ/BHPC//$K_4[Fe(CN)_6]$ AOFB before and after 200 charge-discharge cycles at 20 mA cm^{-2}.

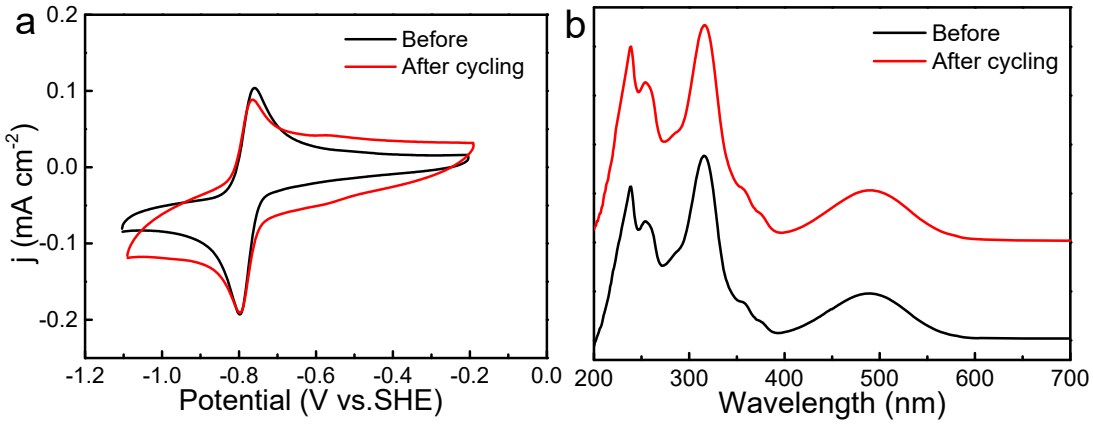

Fig. S11. CVs (a) and UV-vis spectra (b) of BHPC used in the DBPZ/BHPC//$K_4[Fe(CN)_6]$ AOFB before and after 200 charge-discharge cycles at 20 mA cm^{-2}.

Table S2. The comparison of the cycling performance between this work and other reported alkaline AOFBs with organic anolyte materials. CRPC, Capacity retention per cycle. 2,6-DHAQ, 2,6-dihydroxyanthraquinone. 1,8-DHAQ, 1,8-dihydroxyanthraquinone. 2,5-DHBQ, 2,5-dihydroxy-1,4-benzoquinone. 2,6-DBEAQ, 4,4′-((9,10-anthraquinone-2,6-diyl)dioxy) dibutyrate. 2,3-HCNQ, 2-hydroxy-3-carboxy-1,4-naphthoquinone. AMA, alizarin-3-methyliminodiacetic acid. NQ-SO, a mixture of NQ-S and lawsone. DMBQ, 2,5-dihydroxy-3,6-dimethyl-1,4-benzoquinone. DCDHAQ, 1,8-dihydroxy-2,7-dicarboxymethyl-9,10-anthraquinone. 1,3,5,7-THAQ, 1,3,5,7-tetrahydroxyanthraquinone. AQDP, 9,10-anthraquinone-2,6-dipropionic acid. ACA, alloxazine 7/8-carboxylic acid. FMN, flavin mononucleotide. DHPS, 7,8-dihydroxyphenazine-2-sulfonic acid. BHPC, benzo[a]hydroxyphenazine-7/8-carboxylic acid. 1,8-PFP, 3,3'-(phenazine-1,8-diyl)dipropionic acid. AADA, 4-amino-1,1'-azobenzene-3,4′-disulfonic acid. DBPZ, 1,2:3,4-dibenzophenazine.

alkaline AOFB	CRPC	Reference
2,6-DHAQ/$K_4Fe(CN)_6$	99.9% (100 cycles at 100 mA cm^{-2})	[S5]
1,8-DHAQ/$K_4Fe(CN)_6$	99.88% (100 cycles at 80 mA cm^{-2})	[S6]
2,5-DHBQ//$K_4[Fe(CN)_6]$	99.76% (150 cycles at 100 mA cm^{-2})	[S7]
2,6-DBEAQ//$K_4[Fe(CN)_6]$	99.999% (250 cycles at 100 mA cm^{-2})	[S8]
2,3-HCNQ//$K_4[Fe(CN)_6]$	99.95% (100 cycles at 100 mA cm^{-2})	[S9]
AMA//$K_4[Fe(CN)_6]$	99.96% (350 cycles at 100 mA cm^{-2})	[S10]
NQ-SO//$K_4[Fe(CN)_6]$	99.977% (200 cycles at 100 mA cm^{-2})	[S11]
Bislawsone//$K_4[Fe(CN)_6]$	99.962% (at 100-300 mAcm^{-2})	[S12]
DMBQ//$K_4[Fe(CN)_6]$	99.88% (200 cycles at 60 mA cm^{-2})	[S13]
DCDHAQ//$K_4[Fe(CN)_6]$	~99.998% (1360 cycles at 50 mA cm^{-2})	[S14]
1,3,5,7-THAQ//$K_4[Fe(CN)_6]$	99.996% (1100 cycles at 100 mA cm^{-2})	[S15]
AQDP//$K_4[Fe(CN)_6]$	99.9997% (350 cycles at 30 mA cm^{-2})	[S16]
ACA/$K_4Fe(CN)_6$	99.95% (50 cycles at 100 mA cm^{-2})	[S17]
FMN//$K_4[Fe(CN)_6]$	99.99% (100 cycles at 50 mA cm^{-2})	[S18]
DHPS//$K_4[Fe(CN)_6]$	99.992% (1500 cycles at 50 mA cm^{-2})	[S19]
BHPC//$K_4[Fe(CN)_6]$	99.9985% (1305 cycles at 100 mA cm^{-2})	[S20]
1,8-PFP//$K_4[Fe(CN)_6]$	~100% (660 cycles at 20 mA cm^{-2})	[S21]
AADA//$K_4[Fe(CN)_6]$	99.95% (500 cycles at 40 mA cm^{-2})	[S22]
DBPZ-anode-boosted BHPC//$K_4[Fe(CN)_6]$	99.974% (200 cycles at 20 mA cm^{-2})	This work

References

[S1] K. Sato, R. Ichinoi, R. Mizukami, T. Serikawa, Y. Sasaki, J. Lutkenhaus, H. Nishide and K. Oyaizu, J. Am. Chem. Soc. 2018, 140, 1049.

[S2] Y, Zhang, J. Cao, Z. Chen, J. Xu, C. Yu, J. Mater. Chem. A, 2020, 8, 6874.

[S3] J. Luo, A. Sam, B. Hu, C. DeBruler, X. Wei, W. Wang and T. L. Liu, Nano

Energy 2017, 42, 215.

[S4] P. Zhu, P. Tian, T. Gao, H. Pang, J. Ye and G. Ning, Chem. Phys. Lett., 2020, 740: 137080.

[S5] K. Lin, Q. Chen, M. R. Gerhardt, L. Tong, S. B. Kim, L. Eisenach, A. W. Valle, D. Hardee, R. G. Gordon, M. J.Aziz, M. P. Marshak, Science 2015, 349, 1529-1532.

[S6] J. Cao, M. Tao, H. Chen, J. Xu, Z. Chen, J. Power Sources 2018, 386, 40-46.

[S7] Z. J. Yang, L. C. Tong, D. P. Tabor, E. S. Beh, M. A. Goulet, D. De Porcellinis, A. Aspuru-Guzik, R. G. Gordon, M. J. Aziz, Adv. Energy Mater. 2018, 8, 1702056.

[S8] D. G. Kwabi, K. Lin, Y. Ji, E. F. Kerr, M.-A. Goulet, D. De Porcellinis, D. P. Tabor, D. A. Pollack, A. Aspuru-Guzik, R. G. Gordon, M. J. Aziz, Joule 2018, 2, 1907.

[S9] C. Wang, Z. Yang, Y. Wang, P. Zhao, W. Yan, G. Zhu, L. Ma, B. Yu, L. Wang, G. Li, J. Liu, Z. Jin, ACS Energy Lett. 2018, 3, 2404-2409.

[S10] Y. Liu, S. Lu, S. Chen, H. Wang, J. Zhang, Y. Xiang, ACS Appl. Energy Mater. 2019, 2, 2469-2474.

[S11] W. Lee, G. Park, Y. Kwon, Chem. Eng. J. 2019, 386, 123985.

[S12] L. Tong, M.-A. Goulet, D. P. Tabor, E. F. Kerr, D. De Porcellinis, E. M. Fell, A. Aspuru-Guzik, R. G. Gordon, M. J. Aziz, ACS Energy Lett. 2019, 4, 1880-1887.

[S13] P. Sun, Y. Liu, Y. Li, M. A. Shehzad, Y. Liu, P. Zuo, Q. Chen, Z. Yang, T. Xu, Ind. Eng. Chem. Res. 2019, 58, 3994-3999.

[S14] M. Wu, M. Bahari, E. M. Fell, R. G. Gordon, M. J. Aziz, J. Mater. Chem. A, 2021, 9, 26709-26716.

[S15] C. Wang, Z. Yang, B. Yu, H. Wang, K. Zhang, G. Li, Z. Tie, Z. Jin, J. Power Sources 2022, 524, 231001.

[S16] Y. Jing, E. M. Fell, M. Wu, S. Jin, Y. Ji, D. A. Pollack, Z. Tang, D. Ding, M. Bahari, M.-A. Goulet, T. Tsukamoto, R. G. Gordon, M. J. Aziz, ACS Energy Lett. 2022, 7, 226-235.

[S17] K. X. Lin, R. Gomez-Bombarelli, E. S. Beh, L. C. Tong, Q. Chen, A. Valle, A. Aspuru-Guzik, M. J. Aziz, R. G. Gordon, Nat. Energy 2016, 1, 16102-16110.

[S18] A. Orita, M. Verde, M. Sakai, Y. S. Meng, Nat. Commun. 2016, 7, 13230.

[S19] A. Hollas, X. Wei, V. Murugesan, Z. Nie, B. Li, D. Reed, J. Liu, V. Sprenkle, W. Wang, Nat. Energy 2018, 3, 508-514.

[S20] C. Wang, X. Li, B. Yu, Y. Wang, H. Wang, H. Lin, J. Ma, G. Li, Z. Jin, ACS Energy Lett. 2020, 2, 411-417.

[S21] J. Xu, S. Pang, X. Wang, P. Wang, Y. Ji, Joule 2021, 5, 2437-2449.

[S22] X. Zu, L. Zhang, Y. Qian, C. Zhang, G. Yu, Angew. Chem. Int. Ed. 2020, 59, 22163-22170.